Self-consistent calculations of fission barriers in the Fm region

M. Warda,[1,2] J. L. Egido,[1] L. M. Robledo,[1] and K. Pomorski[2,3]

[1]*Departamento de Física Teórica C-XI, Universidad Autónoma de Madrid, Madrid, Spain*
[2]*Katedra Fizyki Teoretycznej, Uniwersytet M. C. Skłodowskiej, Lublin, Poland*
[3]*IReS-IN₂P₃-CNRS and Université Louis Pasteur, Strasbourg, France*

The fission barriers of the nuclei ^{254}Fm, ^{256}Fm, ^{258}Fm, ^{258}No, and ^{260}Rf are investigated in a fully microscopic way up to the scission point. The analysis is based on the constrained Hartree-Fock-Bogoliubov theory and Gogny's D1S force. The quadrupole, octupole, and hexadecapole moments as well as the number of nucleons in the neck region are used as constraints. Two fission paths, corresponding to the bimodal fission, are found. The decrease with isotope mass of the half-life times of heavy Fm isotopes is also explained.

I. INTRODUCTION

As a result of the loss of stability, with respect to spontaneous fission, the number of elements is limited to only a few more than 110. Both experimental and theoretical studies of spontaneous-fission properties are crucial for understanding the stability properties of the heaviest elements. The abrupt transition that occurs from ^{254}Fm to ^{258}Fm in fission-fragment mass and kinetic-energy distributions and in the spontaneous fission half-lives of heavy nuclei was found experimentally (see, e.g., the review articles in [1,2]). For ^{258}Fm and heavier isotopes, the spontaneous-fission half-life decreases relative to ^{256}Fm by several orders of magnitude. The mass distribution of fission fragments of ^{258}Fm becomes very narrow with a single peak at symmetrical fission and the kinetic-energy distribution has two peaks: one at high energy (230 MeV) and the second less prominent at lower energy (205 MeV). On the other hand, the ^{256}Fm isotope exhibits a rather strong mass asymmetric distribution $\bar{A}_L/\bar{A}_H = 112/141$ and only the low-energy peak is observed in the kinetic-energy distribution. This is a rather puzzling situation, from a macroscopic point of view, as a substantial change in the properties of both isotopes is not expected. Therefore, the different fission properties of both isotopes have to be attributed to subtle shell effects, making its theoretical explanation even more challenging.

A qualitative explanation of all these phenomena by the existence of an additional fission valley in the multidimensional potential energy surface was proposed by Hulet *et al.* [3,4]. They assumed a bimodal character of the kinetic-energy and mass distributions to show that for ^{258}Fm there should exist two different fission paths leading to two distinctly different scission configurations. The first one is the conventional scission configuration of two fairly elongated shapes corresponding to the low-kinetic-energy peak and the broad mass distribution. The second one leads to compact scission, i.e., a configuration of two touching spheres corresponding to the high-energy peak in the kinetic-energy distribution and the narrow peak in the mass distribution at symmetric fission.

After the discovery of bimodal fission in ^{258}Fm [3,4], a number of theoretical papers have focused on this problem

[5–11]. All these papers are based on the mean-field single-particle potential and the Strutinsky shell correction method. Most of them deal with the form of the potential-energy surface only. These static calculations usually give two fission valleys: one leading to the elongated form of fission fragments (EFs) and the second one which corresponds to two nearly spherical fragments, which is usually referred as the compact fission (CF) valley. It has been pointed out by Brosa *et al.* [5] that this new CF valley is associated with the doubly magic ($Z=50$, $N=82$) shell closure in the fission fragments.

The macroscopic-microscopic calculations of the potential-energy surface (PES) for ^{258}Fm reported in Ref. [8] are based on the Woods-Saxon single-particle Hamiltonian. The collective potential-energy surface $V(\beta,\beta_4)$ was minimized there with respect to the deformation parameters β_3, β_5, and β_6. Two fission valleys were found, bifurcating right after the exit from the fission barrier. It was also shown in [8] that for the largest values of β ($\beta=1.6$) the EF valley corresponds again to symmetric fission ($\beta_3=\beta_5=0$). This theoretical result is in line with the observation of Hulet *et al.* [3,4] where they found symmetric fission only and equal fission half-life times for both fission modes, i.e., for the fragments with a large total kinetic energy (CF valley) and for those with a small total kinetic energy (EF valley).

Contrary to the estimates of Ref. [8], the results obtained by Möller *et al.* [6,9,12] indicate the existence of the second barrier on the EF path. The authors have found even a third *switchback* path going from the SF valley via the second saddle to the EF valley. These calculations are based on the finite-range liquid drop model and the folded-Yukawa single-particle potential. Additionally, in Refs. [6,9] a smaller mass parameter is postulated along the CF path in order to obtain the comparable spontaneous fission half-life time for both fission modes of ^{258}Fm. In Refs. [10,11] Möller *et al.* tried to find a solution to this problem by making calculations on a five-dimensional space using a finite-range liquid droplet model. They have also found two paths leading to fission, but the low-energy mode was presented as an asymmetric one, with mass asymmetry $M_H/M_L=152.2/105.8$, which does not agree with the experimental data. It was shown in [3,4] that in ^{258}Fm both modes of fission only lead to a symmetric split of the nucleus.

There are also some estimates of fission barriers made within the constrained Hartree-Fock-Bogoliubov (HFB) approximation with Gogny or Skyrme effective interactions both at zero spin [13–21] and at high spin [22]. Most of these calculations were made for nuclei with $Z < 100$, where only the traditional fission path (EF) appears in the experimental data. In [21] calculations for $Z > 100$ showing the compact fission path (CF) were carried out for both nonrelativistic (Skyrme interaction with the SkI4 parameters) and relativistic (in the context of the relativistic mean field with the PL-40 parametrization) frameworks.

Recapitulating we can say that nuclei in the Fm region represent a very wide variety of fission types. The low-mass isotopes fission with an asymmetric mass distribution of the fragments. The spontaneous fission half-life (T_{sf}) increases from about 0.8 ms for ^{242}Fm up to 126 yr for ^{252}Fm and then falls down again to 0.36 ms for ^{258}Fm in order to grow again by one order of magnitude for ^{260}Fm. The situation changes especially dramatically when one goes from ^{256}Fm to ^{258}Fm. The fission half-life decreases by seven orders of magnitude and reaches 0.36 ms and, as was described above, a very narrow symmetric mass distribution appears in the fission yield. Moreover, a similar behavior characterizes heavier nuclei in the neighborhood of ^{258}Fm. Up to now this rapid change of systematics of T_{sf} has not been well described theoretically [11,25].

The aim of the present investigation is to look at the form of the fission barriers obtained with Gogny forces for the nucleus ^{256}Fm and its neighbors. In particular our aim is to answer the following questions:

(i) Do there exist two fission valleys for nuclei in this region?

(ii) Is it possible to reproduce the experimental mass distributions of the fission fragments?

(iii) Is it possible to explain the rapid change of the measured fission half-life between ^{256}Fm and ^{258}Fm?

In order to answer the above questions we have performed constrained Hartree-Fock-Bogoliubov calculations as described in Sec. II, where we give a brief outline of the theoretical model as well as a description of the forces and configuration space. In Sec. III we discuss the results obtained. Section IV contains a summary and some concluding remarks.

II. THEORETICAL MODEL

The Gogny density-dependent effective nucleon-nucleon force is taken in the following form [26]:

$$V_{12} = \sum_{i=1}^{2} (W_i + B_i \hat{P}_\sigma - H_i \hat{P}_\tau - M_i \hat{P}_\sigma \hat{P}_\tau) e^{-(\vec{r}_1 - \vec{r}_2)^2/\mu_i^2}$$

$$+ i W_{LS}(\overleftarrow{\nabla_1 - \nabla})_2 \times \delta(\vec{r}_1 - \vec{r}_2)(\overrightarrow{\nabla_1 - \nabla_2}) \cdot (\vec{\sigma}_1 + \vec{\sigma}_2)$$

$$+ t_0(1 + x_0 \hat{P}_\sigma) \delta(\vec{r}_1 - \vec{r}_2) \left[\rho\left(\frac{\vec{r}_1 + \vec{r}_2}{2}\right) \right]^\gamma + V_{\text{Coul}},$$

$$(2.1)$$

which contains a central finite-range interaction, a zero-range spin-orbit term, and a zero-range density-dependent interaction, respectively. The Coulomb interaction has to be added in the case of protons. The central interaction is a sum of two Gaussian with widths μ_1 and μ_2. Here $\hat{P}\sigma$ and $\hat{P}\tau$ denote the spin and isospin exchange operators, respectively, and ρ is the total density.

We use the D1S [15,27] parametrization of the Gogny interaction. The D1S parameters were adjusted [15] to give a better surface energy term (crucial for a proper description of the fission phenomenon) and their numerical values are given by

$$W_1 = -1720.30 \quad \text{MeV}, \quad W_2 = 103.639 \quad \text{MeV},$$

$$B_1 = 1300.00 \quad \text{MeV}, \quad B_2 = -163.483 \quad \text{MeV},$$

$$H_1 = -1813.53 \quad \text{MeV}, \quad H_2 = 162.812 \quad \text{MeV},$$

$$M_1 = 1397.60 \quad \text{MeV}, \quad M_2 = -223.934 \quad \text{MeV},$$

$$\mu_1 = 0.7 \quad \text{fm}, \quad \mu_2 = 1.2 \quad \text{fm},$$

$$t_0 = 1390.6 \quad \text{MeV fm}^{3(1+\gamma)}, \quad x_0 = 1,$$

$$\gamma = 1/3, \quad W_{LS} = 130 \quad \text{MeV fm}^5. \quad (2.2)$$

The choice of the Gogny force with the D1S parametrization is based on the fact that whenever this interaction has been used to describe low-energy nuclear structure phenomena an, at least, reasonable agreement with experiment has always been obtained. This degree of agreement has been obtained for both calculations at the mean-field level and beyond [26,15–18,22,27–37].

In the microscopic HFB calculations we have used the computer code of [38] where special attention was paid to an accurate computation of the matrix elements of the Gogny interaction for very big bases like the ones used in this paper. The self-consistent equations have been solved by expanding the quasiparticle creation and annihilation operators on finite bases of axially symmetric deformed harmonic oscillator (HO) eigenfunctions. The size of the bases used depends upon two parameters N_0 and q, which are related to the allowed range of the HO quantum numbers through the relation

$$\frac{1}{q} n_z + (2n_\perp + |m|) \leq N_0.$$

Along the perpendicular direction we take N_0 shells (i.e., $2n_\perp + |m| = 0, \ldots, N_0$) and along the z direction we include up to qN_0 shells depending on the value of $2n_\perp + |m|$. In the present study we have used $q = 1.5$, a value which is suited for the elongated shapes along the z direction typical of the fission process, and $N_0 = 13$, 15, and 17. The reason to use different values of N_0 is to study the convergence of our results with the basis size. Other parameters characterizing the HO bases are the oscillator lengths $b_\perp$ and b_z. These two quantities have been determined, for each calculated wave function, so as to minimize the HFB energy for the $N_0 = 13$

basis. The same values of $b_\perp$ and b_z are then used in subsequent calculations with $N_0 = 15$ and 17 (see below for a discussion of the convergence).

To study triaxiality effects in the first fission barrier we have also carried out calculations where the axial symmetry requirement was released but left-right symmetry was imposed. As these calculations are much more time consuming than the axially symmetric ones we had to restrict them to the $N_0 = 13$ case but, as will be discussed later, this is not a limitation in the region of interest.

In order to study the different paths to fission we have used in our calculations the following constraints: the axial quadrupole (Q_2), octupole (Q_3), and hexadecapole (Q_4) moments as well as the number of nucleons in the neck region (Q_N). The corresponding operators are given by

$$\hat{Q}_\lambda = r^\lambda P_\lambda(\cos(\theta)), \quad \hat{Q}_N = \exp\left(\frac{-z^2}{a_N^2}\right), \quad (2.3)$$

with $a_N = 1$ fm.

In the minimization process neither the two-body kinetic-energy correction nor the Coulomb and spin-orbit pairing energies have been taken into account. Additionally, the Coulomb exchange energy has been treated in the Slater approximation [35,39]. The reasons are the following: First, the calculation of the Coulomb exchange and pairing energies is extremely time consuming [35] and its inclusion would prevent the large-scale calculations presented in this paper. From [35] we know that Coulomb pairing can be very important for collective masses but has little influence on the energy landscape. On the other hand, the Slater approximation to the Coulomb exchange energy works fairly well in all cases (spherical or deformed nuclei) and is an affordable and reliable approximation. Concerning the spin-orbit pairing its contribution to the pairing field is very small, especially at zero spin, and can be safely neglected. Finally, the two-body kinetic energy correction (2b-KEC) is not included in the variation process because, for heavy nuclei, it remains almost constant for most of the physical configurations. As this term was included in the fitting of the force, we have to include its contribution at the end of the calculation in order to obtain reasonable binding energies.

We have also subtracted from the HFB energy the rotational energy corrections (RECs) stemming from restoration of the rotational symmetry. This correction has a considerable influence on the energy landscape (and therefore on the height of the fission barriers) as it is somehow proportional to the degree of symmetry breaking and therefore proportional to the quadrupole moment. A full calculation of the RECs would imply an angular momentum projection [36,37] which is only feasible for light nuclei. In order to estimate the RECs we have followed the usual recipe [40] of subtracting to the HFB energy the quantity $\langle \Delta \vec{J}^2 \rangle / (2 \mathcal{J}_Y)$, where $\langle \Delta \vec{J}^2 \rangle$ is the fluctuation associated with the angular momentum operators in the HFB wave function and $\mathcal{J}_Y$ is the Yoccoz moment of inertia [40]. This moment of inertia has been computed using the "cranking" approximation in which the full linear response matrix appearing in its expression is re-

placed by the zero-order approximation. The effect of the "cranking approximation" in the Yoccoz moment of inertia was analyzed with the Gogny interaction for heavy nuclei in [22] by comparing it with the one extracted from an angular momentum projected calculation (see also [37] for a comparison in light nuclei). The conclusion is that the exact REC is a factor 0.7 smaller than the one computed with the "cranking" approximation to the Yoccoz moment of inertia for strongly deformed configurations (a similar behavior has been observed for the Thouless-Valatin moment of inertia in [41]). We have taken this phenomenological factor into account in our calculation of the RECs.

In the last section we analyze the spontaneous fission half-life of several Fm isotopes. The analysis was carried out in the standard WKB framework where T_{sf} is given (in seconds) by

$$T_{sf} = 2.86 \times 10^{-21}[1 + \exp(2S)]. \quad (2.4)$$

In this expression S is the action along the Q_2 constrained path which is given by

$$S = \int_a^b dQ_2 \sqrt{2B(Q_2)[V(Q_2) - E_0]}. \quad (2.5)$$

For the collective quadrupole inertia $B(Q_2)$ we have used the adiabatic time dependent Hartree-Fock-Bogoliubov (AT-DHFB) expression computed again in the "cranking" approximation and given by [42]

$$B_{ATDHFB}(Q_2) = \frac{M_{-3}(Q_2)}{M_{-1}^2(Q_2)}, \quad (2.6)$$

with

$$M_{-n}(Q_2) = \sum_{\mu\nu} \frac{|Q_{\mu\nu}^{20}|^2}{(E_\mu + E_\nu)^n}. \quad (2.7)$$

Here $Q_{\mu\nu}^{20}$ is the 20 component of the quadrupole operator $\hat{Q}_2$ in the quasiparticle representation [40] and E_μ are the quasiparticle energies obtained in the solution of the HFB equation.

In the expression for the action the collective potential $V(Q_2)$ is given by the HFB energy (with the 2b-KEC and REC corrections) minus the zero-point energy (ZPE) correction $\epsilon_0(Q_2)$ associated with the quadrupole motion. This ZPE correction is given by

$$\epsilon_0(Q_2) = \frac{1}{2} G(Q_2) B_{ATDHFB}^{-1}(Q_2), \quad (2.8)$$

where

$$G(Q_2) = \frac{M_{-2}(Q_2)}{2M_{-1}^2(Q_2)}. \quad (2.9)$$

Finally, in the expression for the action an additional parameter E_0 is introduced. This parameter can be taken as the HFB energy of the (metastable) ground state. However, it is argued that in a quantal treatment of the problem the ground-
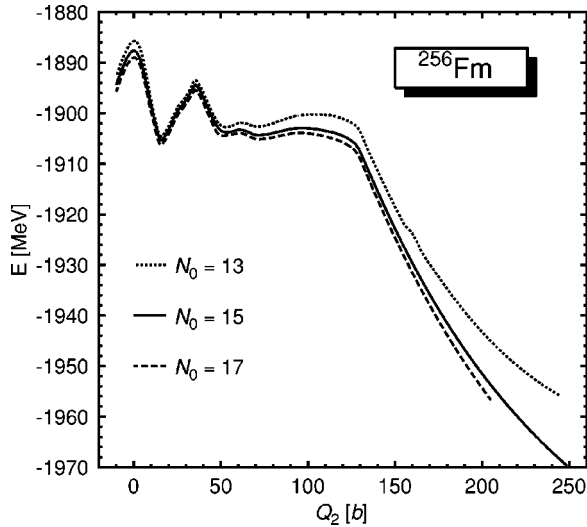
FIG. 1. The HFB energy obtained for $N_0 = 13$, 15, and 17 for the compact fission (CF) path of ^{256}Fm as a function of the quadrupole moment Q_2.
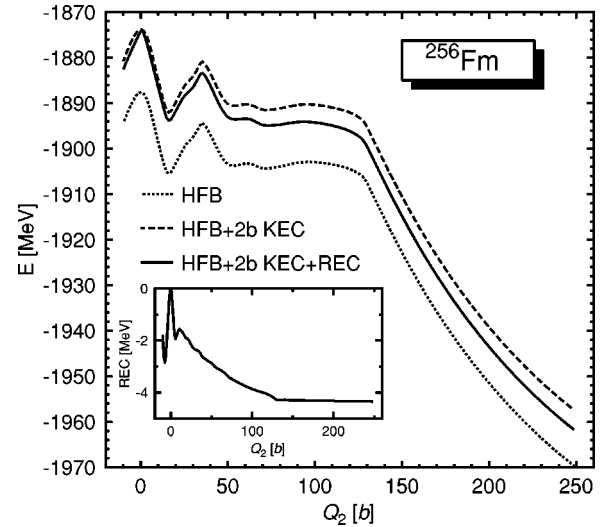

FIG. 2. The potential-energy surface obtained with the HFB calculations (dotted line), the one taking into account the two-body energy correction (dashed line), and the one including also the rotational energy correction (solid line) for the compact fission path of ^{256}Fm as a function of the quadrupole moment Q_2.

state energy is given by the HFB energy plus the zero-point energy associated to the collective motion. To account for this fact, the usual recipe is to add an estimation of the zero-point energy to the HFB energy in order to obtain E_0. In our calculations we have taken a zero-point energy of 0.5 MeV for all the isotopes considered. It is the standard value, but in our opinion the energy E_0 could be considered as an adjustable parameter which shifts the half-lives of neighboring nuclei as a whole.

A. Convergence of the calculations

In our calculations bases with $N_0 = 13$, 15, or 17 were used in order to check the convergence of the results. As an example of these tests we display in Fig. 1 the HFB energies corresponding to the CF path of ^{256}Fm as a function of Q_2 for different values of N_0. A comparison of the $N_0 = 13$ and the $N_0 = 15$ results show that $N_0 = 13$ is enough in the region around the first barrier but this is not the case in the region of the superdeformed minimum, around $Q_2 = 100$ b, where a 4 MeV shift is observed in going from $N_0 = 13$ to $N_0 = 15$.

Using $N_0 = 17$ we obtain rather stable results as compared with the $N_0 = 15$ calculations. That is, for most of the Q_2 range the difference between the $N_0 = 17$ and $N_0 = 15$ energies is almost independent for Q_2. The difference becomes visible only for $Q_2 > 200$ b, but this region is irrelevant to our investigation as it corresponds to solutions with well-separated fragments. This behavior is typical for all paths and nuclei presented in this paper, and from the above considerations, one can conclude that $N_0 = 15$ is sufficient for the planned HFB calculations. We have also checked that this fast convergence with basis size is a consequence of the optimization of the oscillator lengths carried out for each quadrupole deformation. The oscillator length parameters were chosen so as to minimize the HFB energies in the $N_0 = 13$ calculations.

B. Two-body kinetic energy and rotational energy corrections

The influence of the two-body kinetic energy (2b-KEC) and the rotational energy corrections (RECs) on the binding energy and the fission barrier of ^{256}Fm is shown in Fig. 2. It is seen in the figure that the 2b-KEC shifts up the binding energy by around 13 MeV with respect to the HFB estimate, while the REC is negative and its magnitude grows from 0 for the spherical configuration to about 5 MeV in the region of the second barrier (see inset). The plateau observed in the REC starting in $Q_2 = 140$ b is due to the fact that from there on the solution corresponds to two separated spherical fragments. In this case both the moment of inertia and the fluctuation of the angular momentum operators are proportional to the square of the distance between the fragments. As a consequence of the behavior of the REC as a function of the quadrupole moment, its inclusion decreases the second barrier by a few MeV and that has an important influence on the systematics of the spontaneous fission lifetimes of heavy Fm isotopes as will be seen in the next section. All potential-energy surfaces (PESs) presented in this paper contain both the 2b-KEC and REC corrections described above.

III. RESULTS

All nuclei considered here have similar barrier shapes exhibiting two humps. The ground-state minimum is at approximately $Q_2 = 15$ b, which corresponds to the deformation parameter $\beta_2 \approx 0.25$. The first fission barrier is, in our axially symmetric calculations, about 10 MeV high but it is decreased by a few MeV when triaxial shapes are included in the analysis, which is in agreement with results of other authors (consult, e.g., Refs. [24,21]). The lowering of the fission barrier due to triaxiality comes together with an increase of the collective mass and therefore the effect of triaxiality on the fission half-lives is rather small. This is in agreement
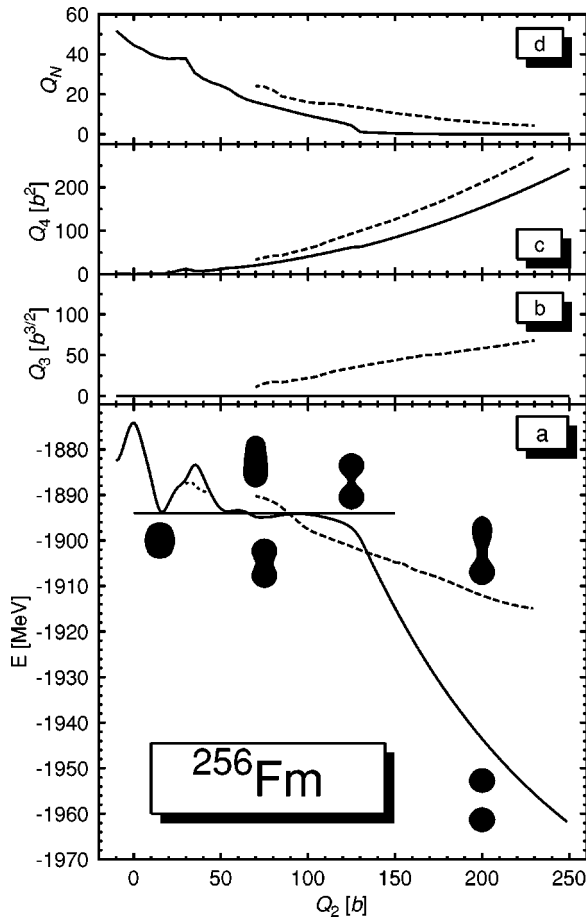
FIG. 3. (a) The fission barrier of ^{256}Fm as a function of the quadrupole moment Q_2 for $N_0 = 15$. The solid line corresponds to the compact fission path (CF) and the dashed line to the elongated one (EF). The dotted line shows the reduction of the first barrier due to nonaxial degrees of freedom. The shapes of the nucleus at a density of $\rho_0 = 0.08$ fm^{-3} are depicted for several values of Q_2 both for the CF and EF paths (note that the EF path leads to octupole deformed shapes). Additionally, in (b), (c), and (d) the octupole and hexadecapole moments as well as the neck parameter Q_N are respectively plotted.

with the results of Ref. [24] where it was found that the least action trajectory, or in other words the dynamical path to fission, leads only through the axially symmetric shapes of the fissioning nucleus. Finally, a superdeformed minimum at an energy similar to the ground-state energy appears at $Q_2 \approx 50$ b. It is separated from the scission point by a small second barrier, which, as we will see in the next section, plays a fundamental role in the fission half-lives.

A. Nuclear properties along the fission paths

In this section the potential energy E, the octupole Q_3, and hexadecapole Q_4 moments as well as the neck parameter Q_N are investigated along the fission paths for the nuclei ^{256,258}Fm, ^{258}No, and ^{260}Rf.

1. ^{256}Fm

In Fig. 3, the results of the calculations for the nucleus

^{256}Fm are plotted for the CF path (solid lines) and the EF path (dashed lines). In panel (a) we show the potential-energy surfaces as a function of the quadrupole moment for both paths. Along with the energy curve we have also plotted the real shape of the nucleus for relevant values of the quadrupole moment. The reduction of the first barrier by approximately 4 MeV due to the triaxial degrees of freedom (γ is typically in the range between $0°$ and $8°$) is marked by the dotted line. We observe that after tunneling through the first barrier the nucleus goes into the superdeformed region. In fact there are two superdeformed minima, one at $Q_2 = 50$ and another at 70 b, separated by a tiny barrier. The deeper minimum at $Q_2 = 70$ b, is situated 2 MeV below the ground-state energy. However, it is only separated from the scission point at $Q_2 = 130$ by a barrier which is only 2 MeV high and therefore it is rather unlikely that this superdeformed (ground state) minimum can live long enough so as to be considered a metastable state. The fission products corresponding to this path are identical and spherical; in fact, the fragments are two spherical ^{128}Sn nuclei. Such a type of fission path (solid line in Fig. 3) was called in Ref. [8] the compact fission (CF) path. It was also shown in [8] that the octupole moment along such a path is equal to zero, which is in line with our results; see panel (b) of Fig. 3. After passing the scission point the potential energy (the Coulomb energy in fact) of this fissioning system decreases rapidly with growing quadrupole moment. The other path, called the elongated fission (EF) path, begins at $Q_2 = 70$ b. This path plays a crucial role in the fission process of this nucleus. It corresponds to the reflection asymmetric shapes with $Q_3 \neq 0$ as one can observe in panel (b) of Fig. 3. Both fission paths differ also significantly in the hexadecapole moments, panel (c), and in the number of nucleons in the neck region, panel (d). For quadrupole moments larger than 120 e b one finds that the EF path has a gentler slope than the CF path.

In order to understand the shapes of the EF path for this nucleus and the heavier isotopes considered we have plotted in panel (a) of Fig. 4 the shape of ^{256}Fm at the deformation $Q_2 = 200$ b. On the left-right asymmetric shape distribution of the fissioning nucleus one can distinguish two fragments connected by a neck. One of the fragments is close to a sphere and the other one has a rather large quadrupole deformation. In order to study the mass contents of both fragments we have plotted in panel (b) the quantity

$$N(z) = 2\pi \int_{-\infty}^{z} dz' \int_{0}^{\infty} dr_\perp \rho(r_\perp, z')$$

for both protons and neutrons. The number of particles corresponding to the magic numbers 50 and 82 is marked in panel (b) with horizontal dotted lines. From this plot we learn that both fragments have roughly the same mass and they correspond to Sn isotopes close to the doubly magic ^{132}Sn. The fact that a strongly left-right asymmetric mass distribution leads to two fragments with roughly the same mass is a remarkable result that will be commented on later. Finally, no significant lowering of the density is observed in the neck region [panel (c) of Fig. 4].
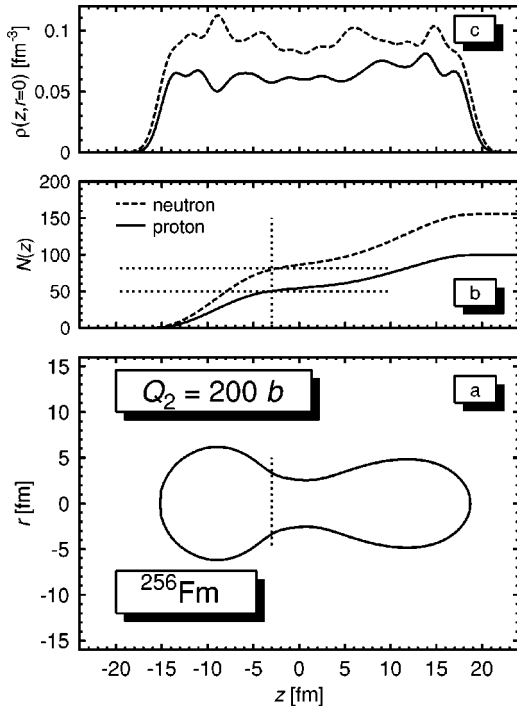
FIG. 4. The shape of ^{256}Fm at deformation $Q_2 = 200$ b on the elongated path to fission as well as the number of particles (b) and the density (c) of protons (solid line) and neutrons (dashed line) as a function of z. The number of particles corresponding to the magic numbers 50 and 82 is marked in panel (b) with horizontal dotted lines.

The transition from the CF to the EF path takes place first at $Q_2 = 90$ b because, for smaller quadrupole moments, the EF path lies on a 5-MeV-high shoulder above the CF path as can be seen in Fig. 5, where cross sections of the potential-energy surface for various quadrupole moments are plotted as a function of the neck parameter Q_N. At $Q_2 = 90$ b the shoulder between both valleys disappears and the nucleus continues to fission along the EF path which becomes deeper for the higher values of Q_2. Such a behavior, referred to by other authors a "switchback path" [12], seems to be energetically most preferable. From $Q_2 = 100$ b up to 130 b the minimum corresponding to the CF valley becomes a shoulder as is seen in Fig. 5. This means that ^{256}Fm cannot continue fissioning along this mode and will proceed through the EF path which explains the low-kinetic-energy distribution of the fission fragments of this nucleus. The minimum corresponding to the CF valley appears again at $Q_2 = 140$ b but at such large quadrupole moments the fragments are already separated. At $Q_2 = 140$ b the fission valleys CF and EF are separated by a 4-MeV-high ridge.

The fragments which are created in the EF process of ^{256}Fm have different deformations but nearly equal masses as seen in Fig. 4. This is inconsistent with the experimental mass distribution which shows a mass asymmetry $A_H / A_L \sim 141/112$ [23]. Our static calculations are based only on the PES of the fissioning nucleus and it seems that dynamical effects could play a certain role in the fission of ^{256}Fm. It could also happen, but this is rather less probable, that we are not able to find such a mass asymmetric path in our calcula-
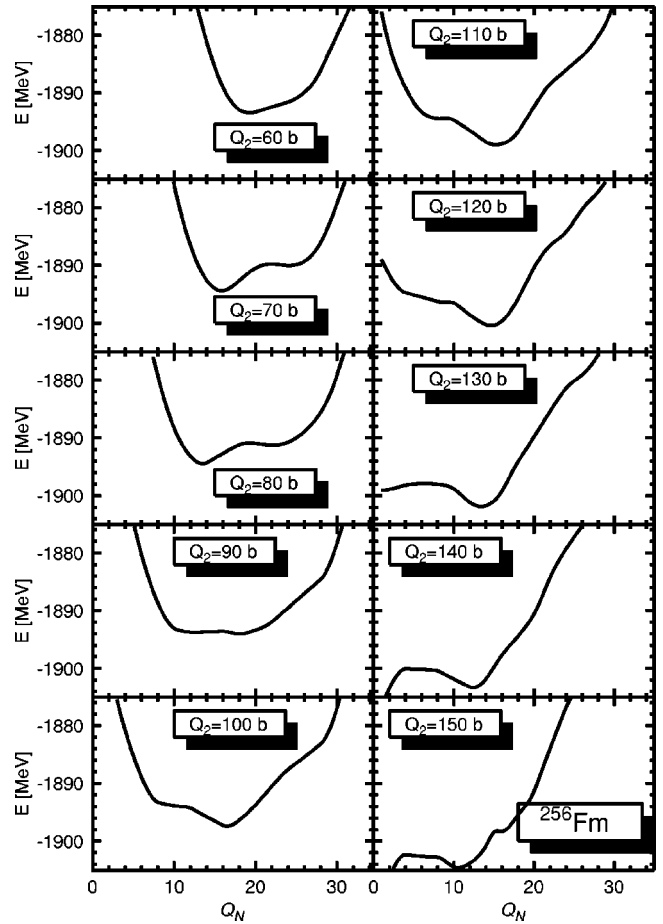

FIG. 5. The cross section of the potential-energy surface of ^{256}Fm for different values of Q_2 as a function of the neck parameter Q_N.

tion. Apart from the two valleys described above a few other paths were found. All of them are localized much above the CF and EF paths so it is rather improbable that the fissioning nucleus will follow one of them.

2. ^{258}Fm

It was found experimentally in Refs. [3,4] that the nucleus ^{258}Fm exhibits bimodal fission. Both modes have a similar abundance and symmetric mass distribution. In panel (a) of Fig. 6 the CF (solid line) and EF (dashed line) fission barriers are shown. The octupole moment, hexadecapole moment, and the number of nucleons in the neck region, Q_N, corresponding to both paths are presented in panels (b)–(d) of Fig. 6. Generally speaking the picture is very similar to the one of ^{256}Fm, but there are some important differences which cause changes in the fission yield of ^{258}Fm.

The first distinction between this nucleus and ^{256}Fm is the fact that the second hump of the fission barrier on the CF path (at $Q_2 = 120$ b) has practically disappeared and rises only 0.5 MeV above the superdeformed minimum. Additionally the top of the second barrier is placed a few MeV below the ground-state energy.

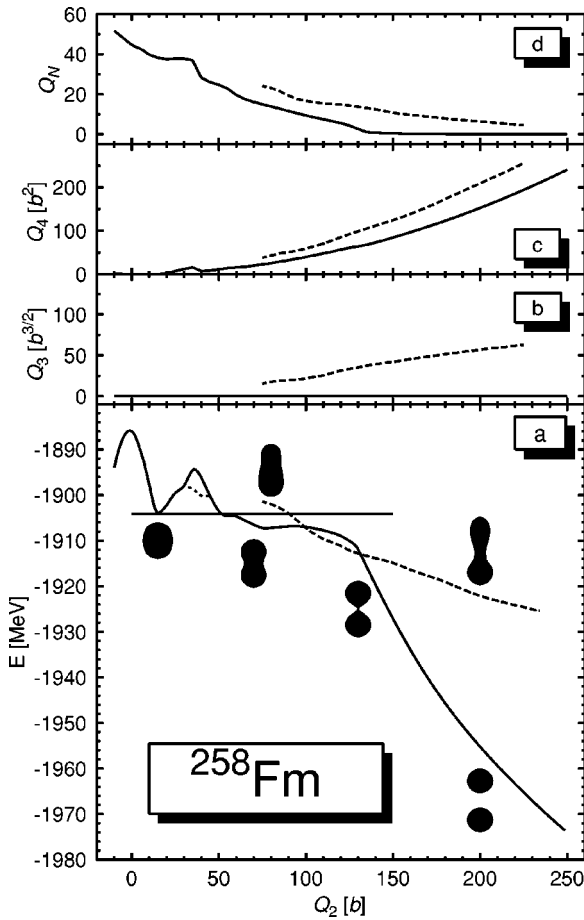The second difference with respect to ^{256}Fm is the relation between the two paths leading to fission. As seen in

FIG. 6. The same as in Fig. 3, but for the ^{258}Fm nucleus.

FIG. 7. The same as in Fig. 5, but for the ^{258}Fm nucleus.

Fig. 7, the minima corresponding to the CF and EF coexist along the fission path; i.e., the ridge between them does not disappear along the whole way to fission. Its height always exceeds 1.5 MeV. It means that the nucleus could fission via the CF valley or change paths and proceed with the EF fragment path starting from $Q_2 \approx 90$ b. At higher quadrupole moments the transfer from the CF to the EF path is also possible but it is less probable as the ridge between the paths in the region of the second hump rises up to 3 MeV. Such a configuration of the EF and CF paths seems to ensure (because we do not account here for dynamical effects) that both modes are fed with similar intensity. This result is in agreement with conclusions of Refs. [3,4], where a comparable abundance of both modes was found.

We can identify the CF path with the high-total-kinetic-energy (TKE) mode in the fission of ^{258}Fm and the EF path with the low-TKE mode. In the CF path the nucleus splits into two identical, spherical parts which are two ^{129}Sn nuclei. At the scission point, the distance between the centers of masses of these spherical fission fragments is relatively small, which gives a strong Coulomb repulsion and in consequence a high mean value of the TKE of the fragments. The fissioning nucleus passing through the second EF path has a similar elongated shape as the one described for ^{256}Fm in Fig. 4. The distance between the mass centers of the two created fragments is much larger than the one for the CF path. It causes a weaker Coulomb repulsion between frag-
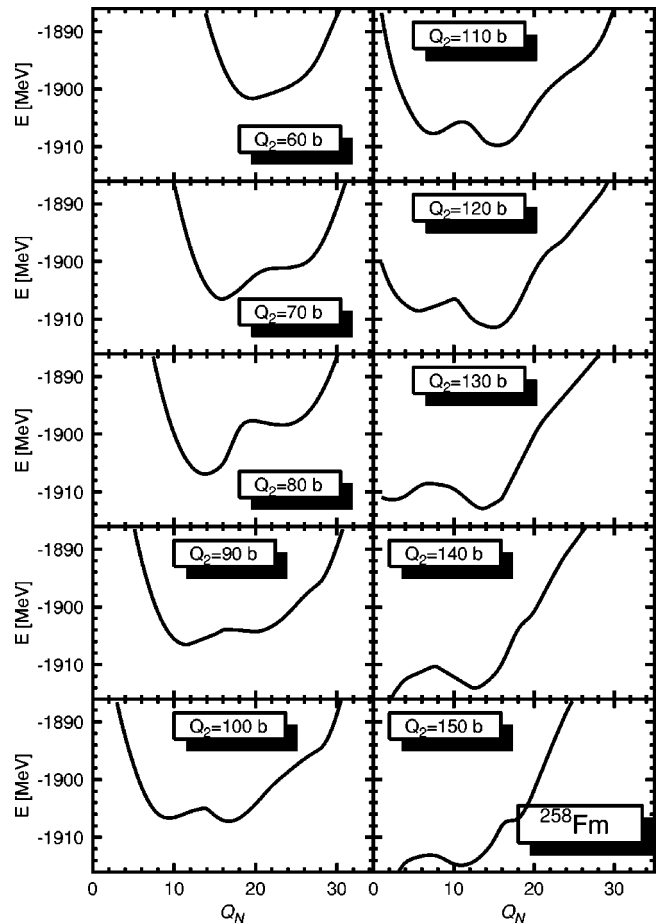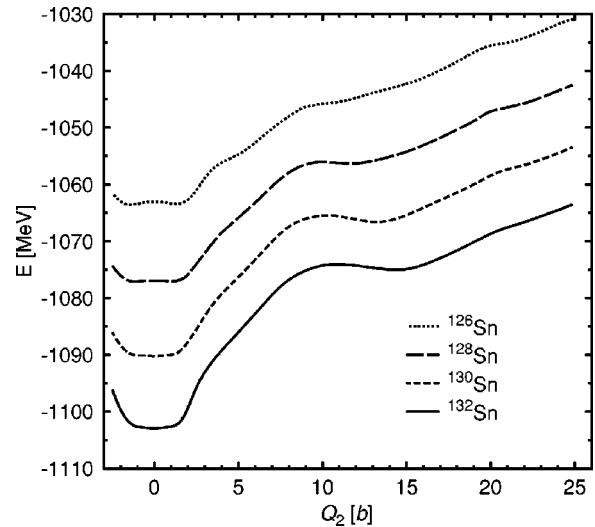

FIG. 8. The potential-energy surfaces for some Sn isotopes as a function of the quadrupole moment Q_2. Both the 2b-KEC and REC are included in the curves.
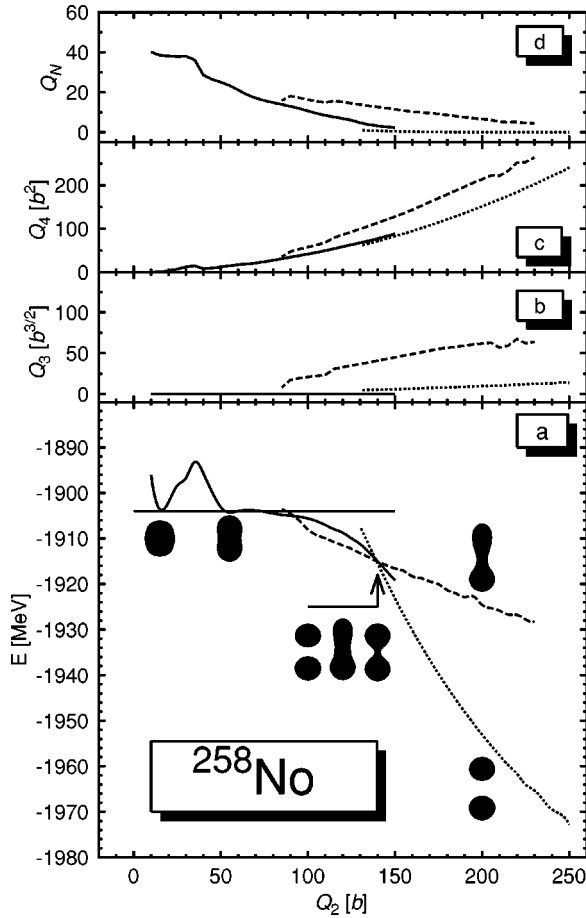
FIG. 9. The same as in Fig. 3, but for the ^{258}No nucleus. The dotted line corresponds to the two-body solution.

FIG. 10. The same as in Fig. 5, but for the ^{258}No nucleus.

ments and in consequence a smaller mean TKE of the fragments.

We have got also some arguments in favor of the hypothesis that in the fission of ^{258}Fm one deals with a kind of cluster fission [2], both in the CF and in the EF paths. Looking at the proton and neutron density distributions along both valleys we have found that the nucleus ^{258}Fm splits into two parts with equal masses. Each fragment has around 50 protons and 79 neutrons. The only difference is that one of the ^{129}Sn fragments created in the EF path is highly deformed with $\beta_2 = 0.6$ whereas it is spherical in the CF path. As the different TKEs of the two paths could be explained in terms of the energy difference between the spherical and superdeformed fragments, we have performed additional Q_2-constrained HFB calculations for a few Sn isotopes. The results for $^{126-132}$Sn even-even isotopes are presented in Fig. 8. A shoulder (or even flat minimum for ^{130}Sn) is seen for all isotopes at $Q_2 = 10-14$ b. This superdeformed second minimum for ^{130}Sn corresponds to $Q_2 = 12$ b (or $\beta_2 = 0.6$) and it is located around 23 MeV above the ground state. This superdeformed state can be identified as the deformed ^{129}Sn fragment, meaning that the 23 MeV accumulated in the superdeformed state will be taken away by post-fission neutrons or γ rays and will not be converted to the kinetic energy of the f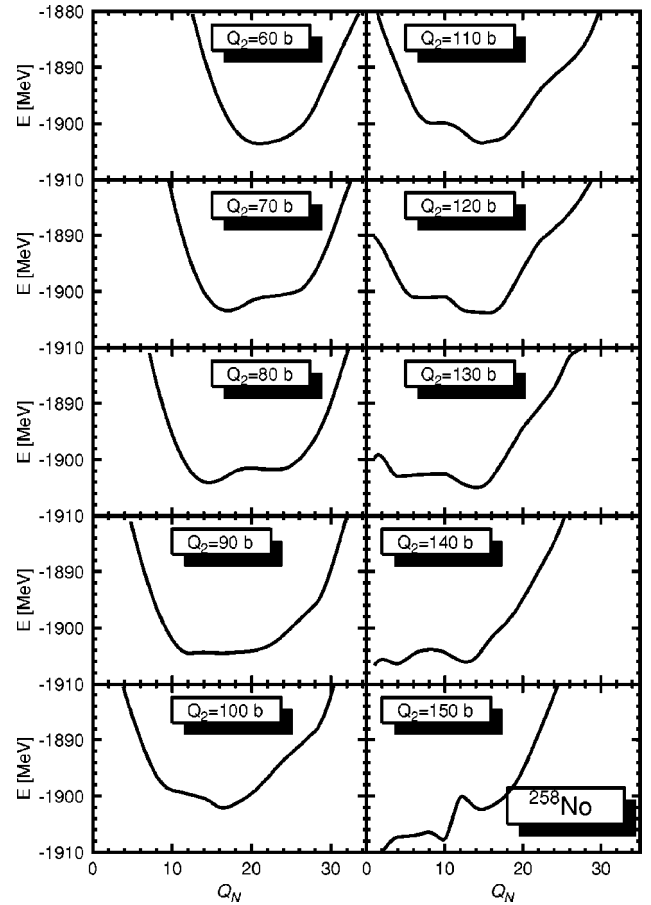ragments. Therefore, we expect that the TKE of the fragments for the EF path to be of the order of 23 MeV smaller than for the CF path, in good agreement with experiment.

3. ^{258}No and ^{260}Rf

Figures 9 and 10 (Figs. 11 and 12) show the PES and its cross sections for the fissioning ^{258}No(^{260}Rf) nucleus. In these nuclei, the second hump of the potential barrier disappears completely. After tunneling through the first barrier they fission directly.

In the nuclei ^{258}No (Fig. 9) and ^{260}Rf (Fig. 11), as in ^{258}Fm, the CF and EF paths are also found. A transition between both valleys is possible at $Q_2 = 90$ b, as can be seen in Figs. 10 and 12, where there is no ridge separating them. Here, similarly to the case of ^{256}Fm, the minimum corresponding to the CF path turns into a shoulder at about $Q_2 = 100$ b, but appears again at $Q_2 = 120-130$ b. It makes possible the comeback to the CF path, although the probability for such a process is relatively small. This effect explains the experimentally observed low abundance of the high-TKE mode: 5% for ^{258}No and even less for ^{260}Rf.

In configurations close to scission another third path corresponding to two compact fragments (marked by the dotted lines in Figs. 9 and 11) will appear. In contrast to the above-considered Fm isotopes, the two fragments have a small asymmetry in mass with a rate of $M_H/M_L = 132.5/125.5$ for
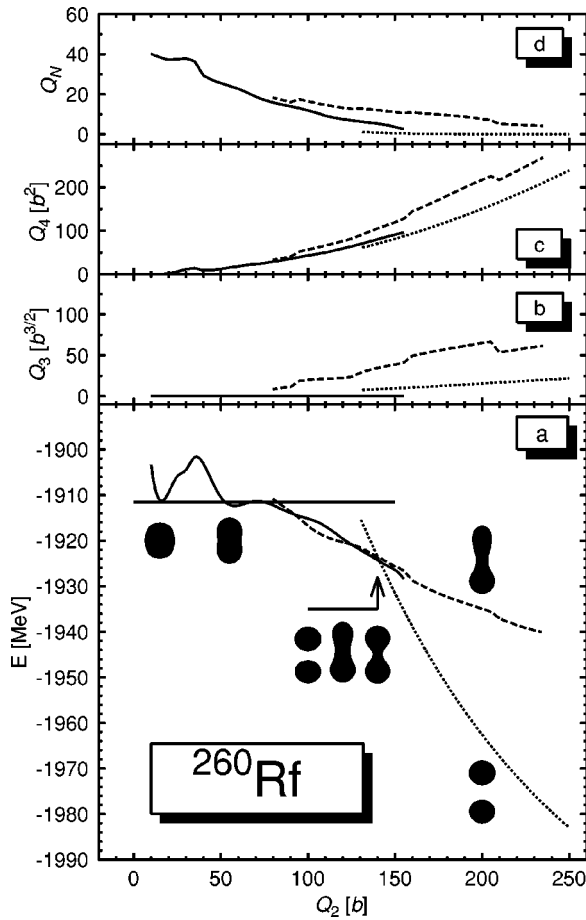
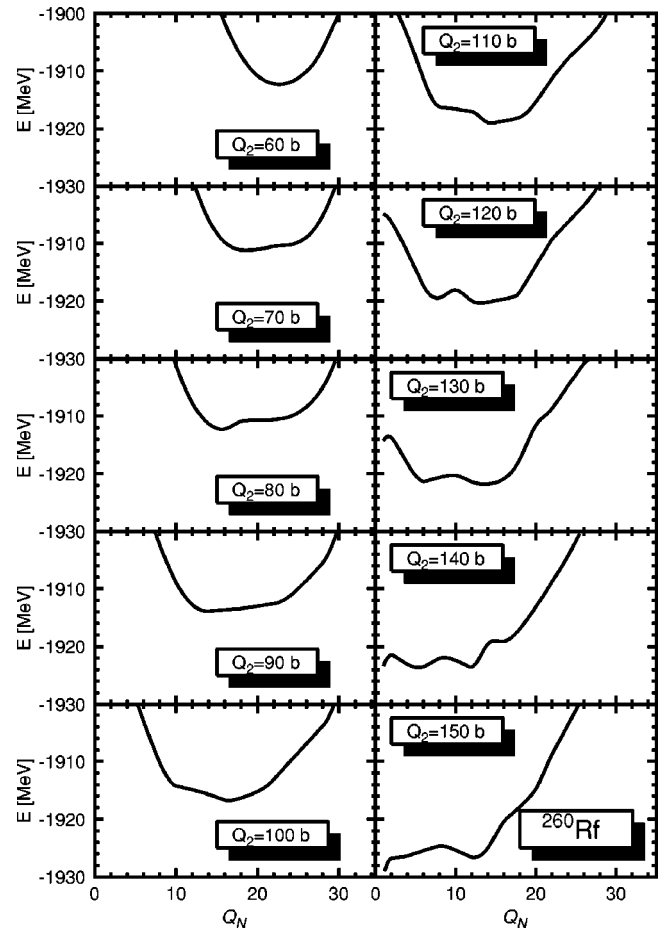FIG. 11. The same as in Fig. 9, but for the ^{260}Rf nucleus.

FIG. 12. The same as in Fig. 5, but for the ^{260}Rf nucleus.

^{258}No and $M_H/M_L = 136/124$ for ^{260}Rf. In both cases the number of protons is the same in both fragments. This asymmetry is in line with the experimental results for these nuclei [3,4].

B. Spontaneous fission half-lives

For heavy Fm isotopes the spontaneous fission half-lives (T_{sf}) decrease rapidly with mass. This falloff has up to now (see, e.g., [25]) not found a satisfactory explanation.

The shape of the potential barrier is one of the most important factors which determines the fission half-life of nuclei. The fission barriers for ^{254}Fm, ^{256}Fm, and ^{258}Fm (for the CF path only) are plotted in Fig. 13. All curves are shifted in order to get the ground-state minimum in the same position. One can see in Fig. 13 that the first hump of the barrier is practically the same for all these nuclei. In fact, the almost 10-MeV-high fission barriers are reduced by a few MeV when including the effect of triaxiality (see Figs. 3 and 6). However, as already mentioned, it was shown in Ref. [24] that the dynamical effect prevents the fissioning nucleus from taking axially nonsymmetric forms, so we have decided to perform the estimates of T_{sf} for the both (axial and non-axial) cases.

The main difference between these three isotopes is in the location of the second hump with respect to the ground-state minimum. In ^{256}Fm the second barrier is at the ground-state

level and in ^{258}Fm a few MeV lower than that. In these nuclei only the first hump will influence the fission half-life time. The fission barrier of ^{254}Fm has a completely different shape. Although the shift up of the second hump with respect to ^{256}Fm is not larger than the corresponding shift in ^{256}Fm with respect to ^{258}Fm, this small shift causes the whole second barrier to be now above the ground state. This effect influences the theoretical estimates for fission half-lives in a dramatical way. The half-life for ^{254}Fm is in our estimates 11 orders of magnitude larger than that for ^{256}Fm when the symmetric (CF) path (solid line in Fig. 3) is taken into account (open symbols in Fig. 14). It becomes much shorter (solid symbols in Fig. 14), and almost equal to the experimental one, when the reduction of the fission barrier due to the left-right asymmetry degrees of freedom is included. It has obviously to do with the fact that the size of the fission barrier to be tunneled in ^{254}Fm reduces slightly if one switches to the EF valley at $Q_2 \approx 90$ b. The estimates done assuming the axially symmetric form of the fissioning nucleus are marked in Fig. 14 by circles, while those for the nonaxial case are denoted by triangles. It is seen that the inclusion of the nonaxial degrees of freedom decreases the values of T_{sf} obtained in our one-dimensional calculation (i.e., without the dynamical effects of Ref. [24]) by about one order of magnitude.
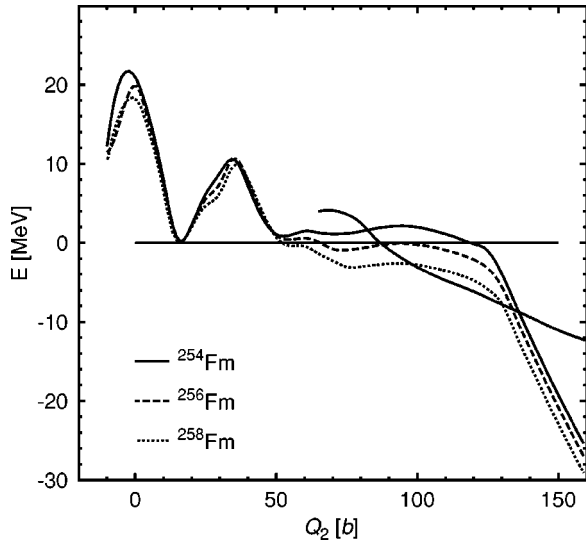
FIG. 13. The fission barriers for ^{254}Fm, ^{256}Fm, and ^{258}Fm evaluated along the CF path. The ground state is set to zero in the three cases. The second solid line starting at $Q_2 = 60$ b corresponds to the EF path of ^{254}Fm.

In Fig. 14 we compare our estimates for the spontaneous fission half-lives (T_{sf}) with the experimental data and also with the results of dynamical calculations on the basis of the Woods-Saxon potential made in Ref. [25]. It is seen that we have qualitatively explained its decrease for heavy Fm isotopes. It is due to the fact that the second hump goes below the ground-state level in $^{256-258}$Fm. In fact, we did not reproduce well enough the half-life time for ^{256}Fm which is in our calculations three orders of magnitude shorter than the measured value and, therefore, the abrupt change in the systematics of the fission lifetimes appears two mass units too early.

IV. CONCLUSIONS

In this paper we have discussed some properties of the potential-energy surfaces of fissioning even-even nuclei in the ^{258}Fm region. All discussed nuclei exhibit two-hump fission barriers. There is always one of the fission trajectories which leads to compact fission. Another path, leading to an alternative mode corresponding to a spherical and an elongated fission fragment, has been found for all these nuclei. The shape of the second hump of the potential barrier and the relation between the two fission paths in the potential-energy surface are crucial for the way in which fission occurs in these nuclei.

In ^{256}Fm fission follows only the elongated fission path but we are unable, in our static calculation, to reproduce properly the mass asymmetry of the fission products of ^{256}Fm. Similarly to the experimental situation the theoretical approach yields only a low-TKE mode in the fission yields, which was found theoretically. In contrast to this, the isotope ^{258}Fm may fission along the CF or EF valleys and bimodal fission take place there. The observed experimental difference of the TKE between both modes is well reproduced by our model. The mechanism of bimodal fission of ^{258}Fm and
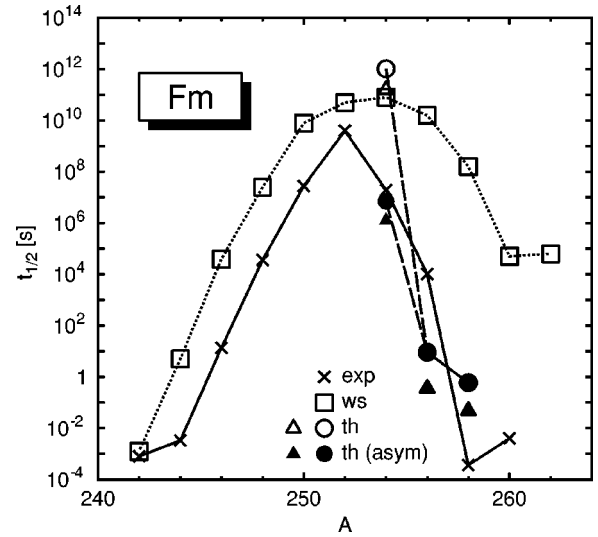

FIG. 14. The spontaneous fission half-life times of Fm isotopes as a function of the mass number. The experimental data (exp) are taken from the NuDat database while the theoretical estimates computed with a model based on the Woods-Saxon (WS) potential are taken from Ref. [25]. The present estimates are represented by solid circles for fission along the CF path whereas the results for fission along the EF path are represented by open circles (note that both estimates coincide in $^{256-258}$Fm). These results were obtained assuming the axial symmetry of a fissioning nucleus. Similar estimates done with the inclusion of nonaxial degrees of freedom are marked by triangles.

the heavier even-even nuclei has been described properly.

We also explained the decrease of the half-life times for the heavy Fm isotopes. In the case of ^{254}Fm, the second hump on the fission barrier is located above the ground state. In heavier isotopes it goes down by a few MeV below the ground-state minimum and therefore does not give any contribution to the half-life times of these nuclei.

Contrary to the majority of papers describing the bimodal fission of ^{258}Fm we have found a strong left-right asymmetry in the shape of a fissioning nucleus which nevertheless corresponds to a symmetric mass split. This is a new phenomenon which could be discovered only in the HFB type of calculations with the Gogny or δ-pairing forces which distinguish between orbitals in different fragments.

[1] D.C. Hoffman, Nucl. Phys. **A502**, 21c (1989).

[2] F. Gönnenwein, Nucl. Phys. **A654**, 855c (1999).

[3] E.K. Hulet, J.F. Wild, R.J. Dougan, R.W. Lougheed, J.H. Landrum, A.D. Dougan, M. Schädel, R.L. Hahn, P.A. Baisden, C.M. Henderson, R.J. Dupzyk, K. Sümmerer, and G.R. Bethune, Phys. Rev. Lett. **56**, 313 (1986).

[4] E.K. Hulet, J.F. Wild, R.J. Dougan, R.W. Lougheed, J.H. Landrum, A.D. Dougan, P.A. Baisden, C.M. Henderson, R.J. Dupzyk, M. Schädel, K. Sümmerer, and G.R. Bethune, Phys. Rev. C **40**, 770 (1989).

[5] U. Brosa, S. Grossmann, and A. Müller, Z. Phys. A **325**, 241 (1986).

[6] P. Möller, J.R. Nix, and W.J. Świątecki, Nucl. Phys. **A469**, 1 (1987).

[7] V.V. Pashkevich, Nucl. Phys. **A477**, 1 (1988).

[8] S. Ćwiok, P. Rozmej, A. Sobiczewski, and Z. Patyk, Nucl. Phys. **A491**, 281 (1989).

[9] P. Möller, J.R. Nix, and W.J. Świątecki, Nucl. Phys. **A492**, 349 (1989).

[10] P. Möller and A. Iwamoto, Phys. Rev. C **61**, 047602 (2000).

[11] P. Möller, D.G. Madland, A.J. Sierk, and A. Iwamoto, Nature (London) **409**, 785 (2001).

[12] P. Möller and J.R. Nix, Nucl. Phys. **A549**, 84 (1992).

[13] J. Bartel, P. Quentin, M. Brack, C. Guet, and H.B. Håkansson, Nucl. Phys. **A386**, 79 (1982).

[14] M. Brack, C. Guet, and H.B. Håkansson, Phys. Rep. **123**, 275 (1985).

[15] J.F. Berger, M. Girod, and D. Gogny, Nucl. Phys. **A428**, 23c (1984).

[16] J.F. Berger, M. Girod, and D. Gogny, Nucl. Phys. **A502**, 85c (1989).

[17] J. F. Berger, L. Bitaud, J. Dechargé, M. Girod, and S. Peru-Dessenfants, in *Proceedings of the International Workshop XXXIV on Gross Properties of Nuclei and Nuclear Excitations*, Hirschegg, Austria, 1996, edited by H. Feldmeier, J. Knoll, and W. Nörenberg (GSI, Darmstadt, 1996), p. 56.

[18] C.R. Chinn, J.F. Berger, D. Gogny, and M.S. Weiss, Phys. Rev. C **45**, 1700 (1992).

[19] S. Ćwiok, J. Dobaczewski, P.-H. Heenen, P. Magierski, and W. Nazarewicz, Nucl. Phys. **A611**, 211 (1996).

[20] K. Rutz, M. Bender, T. Burvenich, P.-G. Reinhard, J.A. Maruhn, and W. Greiner, Phys. Rev. C **56**, 238 (1997).

[21] M. Bender, K. Rutz, P.-G. Reinhard, J.A. Maruhn, and W. Greiner, Phys. Rev. C **58**, 2126 (1998).

[22] J.L. Egido and L.M. Robledo, Phys. Rev. Lett. **85**, 1198 (2000).

[23] R. Vandenbosch and J. R. Huizenga, *Nuclear Fission* (Academic, New York, 1973).

[24] A. Baran, K. Pomorski, A. Łukasiak, and A. Sobiczewski, Nucl. Phys. **A361**, 83 (1981).

[25] A. Staszczak and Z. Łojewski, Nucl. Phys. **A657**, 134 (1999).

[26] J. Dechargé and D. Gogny, Phys. Rev. C **21**, 1568 (1980).

[27] J.F. Berger, M. Girod, and D. Gogny, Comput. Phys. Commun. **63**, 365 (1991).

[28] M. Girod and B. Grammaticos, Phys. Rev. C **27**, 2317 (1983).

[29] J.L. Egido and L.M. Robledo, Nucl. Phys. **A494**, 85 (1989).

[30] M. Girod, J.P. Delaroche, D. Gogny, and J.F. Berger, Phys. Rev. Lett. **62**, 2452 (1989).

[31] J.L. Egido and L.M. Robledo, Phys. Rev. Lett. **70**, 2876 (1993).

[32] J.P. Blaizot, J.F. Berger, J. Dechargé, and M. Girod, Nucl. Phys. **A591**, 435 (1995).

[33] A. Valor, J.L. Egido, and L.M. Robledo, Phys. Rev. C **53**, 172 (1996).

[34] E. Garrote, J.L. Egido, and L.M. Robledo, Phys. Rev. Lett. **80**, 4398 (1998).

[35] M. Anguiano, J.L. Egido, and L.M. Robledo, Nucl. Phys. **A683**, 227 (2001).

[36] R. Rogríguez-Guzmán, J.L. Egido, and L.M. Robledo, Phys. Rev. C **65**, 024304 (2002).

[37] R. Rogríguez-Guzmán, J.L. Egido, and L.M. Robledo, Phys. Rev. C **62**, 054319 (2000); Phys. Lett. B **474**, 15 (2000); Acta Phys. Pol. B **32**, 2385 (2001).

[38] J.L. Egido, L.M. Robledo, and R.R. Chasman, Phys. Lett. B **393**, 13 (1997).

[39] C. Titin-Schnaider and Ph. Quentin, Phys. Lett. **49B**, 213 (1974).

[40] P. Ring and P. Schuck, *The Nuclear Many Body Problem* (Springer-Verlag, Berlin, 1980).

[41] M. Girod, J.P. Delaroche, J. Libert, and I. Deloncle, Phys. Rev. C **45**, R1420 (1992).

[42] M.J. Giannoni and Ph. Quentin, Phys. Rev. C **21**, 2060 (1980).